Journal of Alloys and Compounds 480 (2009) L29–L32

Contents lists available at ScienceDirect

Journal of Alloys and Compounds

journal homepage: www.elsevier.com/locate/jallcom

Letter

Aging-induced, defect-mediated double ferroelectric hysteresis loops and large recoverable electrostrains in Mn-doped orthorhombic $KNbO_3$-based ceramics

Zuyong Feng, Siu Wing Or*

Department of Electrical Engineering, The Hong Kong Polytechnic University, Hung Hom, Kowloon, Hong Kong

ARTICLE INFO

Article history:
Received 20 January 2009
Received in revised form 7 February 2009
Accepted 11 February 2009
Available online 24 February 2009

Keywords:
Aging
Defects
Double ferroelectric hysteresis loop
Lead-free ceramics
Recoverable electrostrains

ABSTRACT

Double ferroelectric hysteresis (P–E) loops and large recoverable electrostrains of >0.13% at 5 kV/mm are observed in aged Mn-doped orthorhombic $KNbO_3$-based [$K(Nb_{0.90}Ta_{0.10})O_3$] lead-free ceramics over a wide temperature range of 25–140 °C. The observations are found to have striking similarities to tetragonal ferroelectrics, besides following a point defect-mediated reversible domain switching mechanism of aging driven by a symmetry-conforming short-range ordering (SC-SRO) of point defects. Such aging effects, being insensitive to crystal structure and constituent ionic species, provide a useful way to enhance electromechanical properties of lead-free ferroelectric material systems.

Aging is a physical phenomenon in many ferroelectric materials characterized by the spontaneous changes of ferroelectric, dielectric, and piezoelectric properties with time [1–4]. This phenomenon is generally detrimental as it tends to limit the application viability of ferroelectrics in terms of reliability and stability. However, a series of recent studies show that the phenomenon is useful and valuable because anomalous double (or constricted) ferroelectric hysteresis (P–E) loops accompanying large recoverable electrostrains can be intentionally induced in impurity- or acceptor-doped tetragonal ferroelectric titanates, such as barium titanate ($BaTiO_3$), after aging [2,5–7]. Importantly, it can manage such aging effects to provide an alternative way to enhance the electromechanical properties of tetragonal ferroelectrics. From the phenomenological respects, the aging effects can be described by a gradual stabilization of the ferroelectric domain structure by defects (i.e., dopant, vacancy or impurity) [8–10], and various stabilization theories, including the grain-boundary theory, surface-layer model, domain-wall theory, and volume theory, were proposed in the past decades [2,11–15]. Among them, the domain-wall-pinning effect was accepted as a general mechanism of aging [2,5]. It is only quite recently that the volume effect based on the symmetry-conforming principle of point defects was recognized as the intrinsic governing mechanism of ferroelectric aging [2,7,16].

Since orthorhombic ferroelectric phase lies widely in ferroelectrics as tetragonal ferroelectric phase, orthorhombic ferroelectrics are interesting and important ferroelectrics as well [17–19]. For instance, orthorhombic $A^+B^{5+}O_3$ alkaline niobates ($KNbO_3$) are promising candidates for lead-free piezoelectric applications because of their good piezoelectric properties and high Curie temperatures [18,19]. In this work, we aim to investigate the aging effects in an Mn-doped orthorhombic $KNbO_3$-based [$K(Nb_{0.90}Ta_{0.10})O_3$] lead-free ceramic: $K[(Nb_{0.90}Ta_{0.10})_{0.99}Mn_{0.01}]O_3$ so as to provide a relatively complete picture about the aging on both orthorhombic and tetragonal ferroelectrics for the related communities.

$K[(Nb_{0.90}Ta_{0.10})_{0.99}Mn_{0.01}]O_3$ ceramic was synthesized using a conventional solid-state reaction technique. This compound was essentially based on $KNbO_3$ but modified by adding 10% Ta to the Nb site. Such modification shifted the phase transition temperatures of cubic–tetragonal (T_C) and tetragonal–orthorhombic (T_{O-T}) to the lower frequency side and made the "hard" material to be relatively "soft" [20]. 1.0 mol.% Mn was added to the B-site of [$K(Nb_{0.90}Ta_{0.10})O_3$] as the acceptor dopant. The starting chemicals were K_2CO_3 (99.5%), Nb_2O_5 (99.9%), Ta_2O_5 (99.9%), and MnO_2 (99%). Calcination was done at 850 °C for 4 h in a K_2O-rich atmosphere, and sintering was carried out at 1050 °C for 0.5 h in air. In order to remove the historical effect, all the as-prepared samples were deaged by holding at 500 °C for 1 h followed by an air-quench to room temperature. The quenched and deaged samples are designated as "fresh samples". Some fresh samples were aged at 130 °C for 5 days, and the resulting samples are denoted as "aged samples". The temperature dependence of dielectric constant of the fresh samples was evaluated at different frequencies using a LCR meter (HIOKI 3532) with a temperature chamber. The bipolar and unipo-

* Corresponding author. Tel.: +852 34003345; fax: +852 23301544.
E-mail address: eeswor@polyu.edu.hk (S.W. Or).

0925-8388/$ – see front matter © 2009 Elsevier B.V. All rights reserved.
doi:10.1016/j.jallcom.2009.02.043

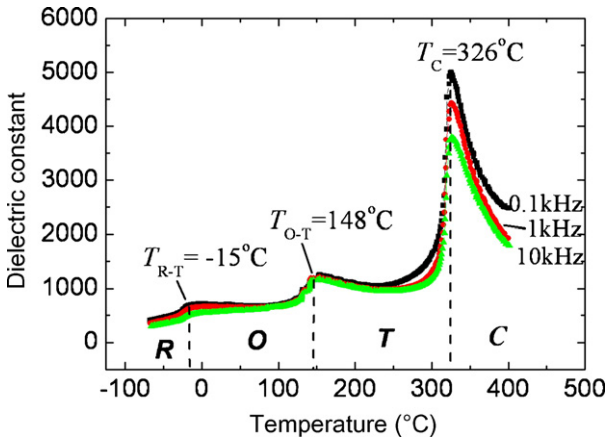

Fig. 1. Temperature dependence of dielectric constant for the fresh samples at the frequencies of 0.1, 1, and 10 kHz. *C* = cubic, *T* = tetragonal, *O* = orthorhombic, and *R* = rhombohedral.

lar ferroelectric hysteresis (*P*–*E*) loops and electrostrain curves for the aged and fresh samples were measured at 5 Hz using a precision ferroelectric test system (Radiant Workstation) and a photonic displacement sensor (MTI 2000) under various temperatures in a temperature-controlled silicon oil bath.

Fig. 1 shows the temperature dependence of dielectric constant for the fresh samples at the frequencies of 0.1, 1, and 10 kHz. Three distinct dielectric peaks are observed at about 326, 148, and −15 °C, respectively. X-ray diffraction (XRD) characterization indicates that they correspond to the phase transition temperatures of cubic (paraelectric)–tetragonal (ferroelectric) (T_C), tetragonal (ferroelectric)–orthorhombic (ferroelectric) (T_{O-T}), and orthorhombic (ferroelectric)–rhombohedral (ferroelectric) (T_{R-O}), respectively [20]. Therefore, our samples have a rhombohedral (*R*) structure for temperatures below −15 °C, an orthorhombic (*O*) structure for temperatures ranging from −15 to 148 °C, a tetragonal (*T*) structure for temperatures varying from 148 to 326 °C, and a cubic (*C*) structure for temperatures above 326 °C.

Fig. 2 illustrates the bipolar and unipolar ferroelectric hysteresis (*P*–*E*) loops and electrostrain curves for the aged and fresh samples at room temperature. In contrast with the normal bipolar *P*–*E* loop for the fresh samples, the aged samples in Fig. 2(a) possess an interesting bipolar double *P*–*E* loop, very similar to that of the aged acceptor-doped tetragonal ferroelectrics such as the $A^{2+}B^{4+}O_3$ system [5–7]. Moreover, a large recoverable electrostrain of 0.15% at 5 kV/mm, accompanying the double *P*–*E* loop, is achieved in our aged samples. This recoverable electrostrain curve is indeed different from the butterfly irrecoverable electrostrain curve as obtained in the fresh samples due to the existence of a recoverable domain switching in the aged samples but an irrecoverable domain switching in the fresh samples. Fig. 2(b) shows the unipolar *P*–*E* loops and electrostrain curves for the aged and fresh samples. It is clear that a large polarization *P* of ~22 μC/cm^2 is obtained at 5 kV/mm for the aged samples compared to a much smaller *P* of ~6 μC/cm^2 in the fresh samples at the same field level. With the large *P*, a large nonlinear electrostrain of 0.15% at 5 kV/mm is available for the aged samples owing to the reversible domain switching. It is noted that this electrostrain not only is 2.5 times larger than the fresh samples, but also exceeds the "hard" lead zirconate titanate (PZT) value of 0.125% at 5 kV/mm [21]. It is also noted that the electrostrain in our fresh samples (having a small quantity of Mn acceptor dopant) is not obviously different from that in the undoped $K(Nb_{0.90}Ta_{0.10})O_3$ ceramic, and similarly large electrostrain has been reported recently on the aged tetragonal $K(Nb_{0.65}Ta_{0.35})O_3$-based ceramics [22].

Although our orthorhombic $K[(Nb_{0.90}Ta_{0.10})_{0.99}Mn_{0.01}]O_3$ ceramic has different crystal symmetry from tetragonal ferroelectric $BaTiO_3$, they all belong to perovskite ABO_3 structure. This lets us to believe that the observed aging effects in our aged orthorhombic samples can be explained according to a point defect-mediated reversible domain switching mechanism of aging driven by a symmetry-conforming short-range ordering (SC-SRO) of point defects (i.e., acceptor ions and vacancies) adopted successfully in $BaTiO_3$ [5–7]. In fact, when acceptor dopant Mn^{4+}/Mn^{3+} ions displace the central Nb^{5+}/Ta^{5+} ions of the *B*-site in the aged $K[(Nb_{0.90}Ta_{0.10})_{0.99}Mn_{0.01}]O_3$ samples, oxygen vacancies V_O form at the O^{2-} sites to maintain the charge neutrality, resulting in point defects (i.e., defect dipoles) with the central acceptor dopants. Fig. 3 depicts how such aging effects are produced in a single-crystal

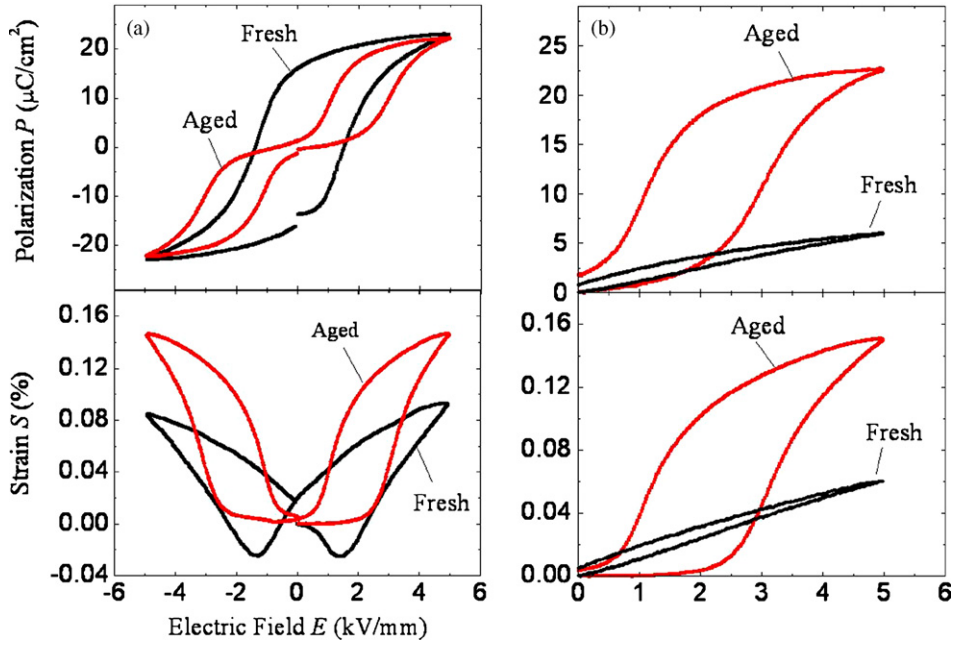

Fig. 2. (a) Bipolar and (b) unipolar ferroelectric hysteresis (*P*–*E*) loops and electrostrain curves for the aged and fresh samples at room temperature.

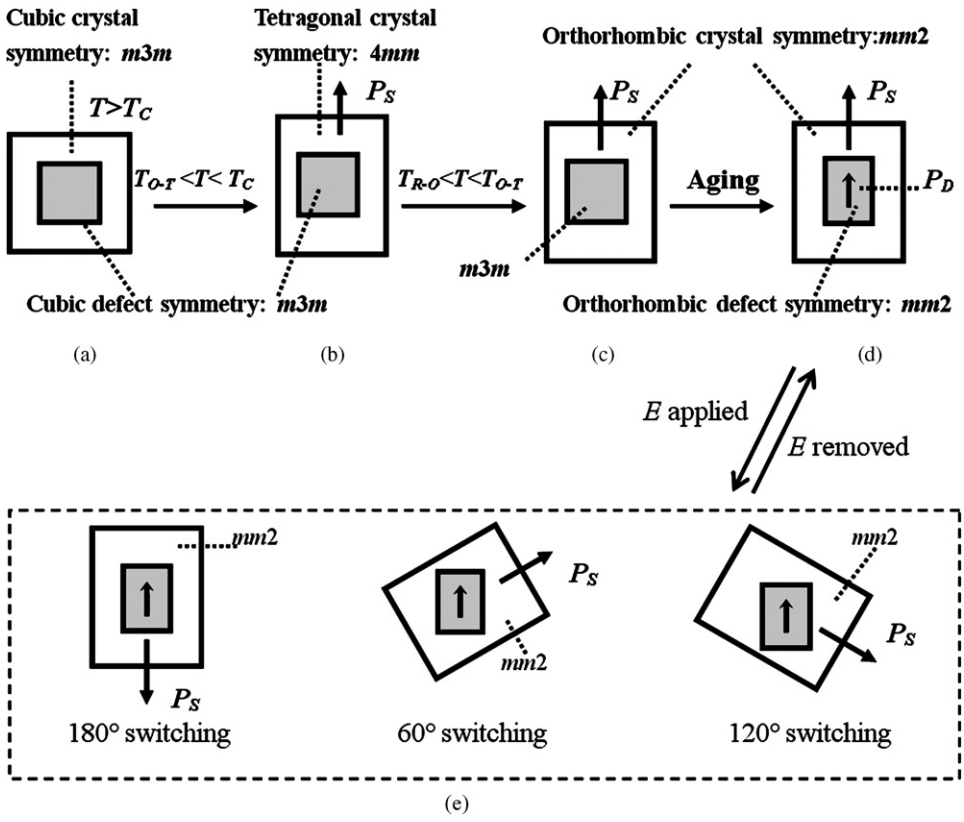

Fig. 3. Crystal and defect symmetries of a single-crystal grain in (a) a fresh $K[(Nb_{0.90}Ta_{0.10})_{0.99}Mn_{0.01}]O_3$ sample at $T > T_C$, (b) the fresh sample at $T_{O-T} < T < T_C$, (c) the fresh sample at $T_{R-O} < T < T_{O-T}$, (d) an aged sample at room temperature, and (e) electric field E-induced switching of the 180°, 60°, and 120° ferroelectric domains in the aged sample at room temperature.

grain of our aged samples. Some associated remarks are included as follows.

(1) When the fresh samples are just sintered and their temperature (T) is still above the Curie point T_C (i.e., $T > T_C$), its single-crystal grain exhibits a cubic crystal symmetry $m3m$, and point defects naturally show a conforming cubic defect symmetry $m3m$, as shown in Fig. 3(a).

(2) At $T_{O-T} < T < T_C$, the single-crystal grain of the fresh samples shows a tetragonal crystal symmetry $4mm$, due to the displacement of positive and negative ions along the [0 0 1] crystallographic axis, producing a nonzero spontaneous polarization P_S as shown in Fig. 3(b). However, the short-range ordering (SRO) distribution of point defects keeps the same cubic defect symmetry $m3m$ as that in the cubic paraelectric phase because the diffusionless paraferroelectric transition cannot alter the original cubic SRO symmetry of point defects [5].

(3) At $T_{R-O} < T < T_{O-T}$, the single-crystal grain of the fresh samples exhibits an orthorhombic crystal symmetry $mm2$, owing to the ferroelectric-ferroelectric phase transition from the tetragonal to orthorhombic structure, producing a nonzero P_S along the [1 1 0] crystallographic axis as shown in Fig. 3(c). Again, the SRO distribution of point defects still keeps the same cubic defect symmetry $m3m$ because of fast cooling. As a result, two unmatched symmetries (i.e., the orthorhombic crystal symmetry and the cubic defect symmetry) exist simultaneously in the fresh ferroelectric state (Fig. 3(c)). According to the SC-SRO principle [23], such a state is energetically unstable and the samples tend to a symmetry-conforming state.

(4) After aging at 130 °C for 5 days in the ferroelectric state, the cubic defect symmetry $m3m$ changes gradually into a polar orthorhombic defect symmetry $mm2$, while the single-crystal grain of the aged samples has a polar orthorhombic crystal symmetry $mm2$, as shown in Fig. 3(d). Such a change is realized by the migration of V_O during aging, and the polar orthorhombic defect symmetry creates a defect polarization P_D, aligning along the spontaneous polarization P_S direction (Fig. 3(d)).

(5) When an electric field E is initially applied in opposition to P_S of the aged orthorhombic samples (Fig. 3(e)), an effective switching of the available 180° ferroelectric domains is induced, contributing to a small polarization at low E (<1.5 kV/mm), as shown in Fig. 2(b). Continuing a larger applied E (>1.5 kV/mm), non-180° domain switching (mainly 60° and 120° domain switching according to the polar orthorhombic crystal symmetry) is induced, but the polar orthorhombic defect symmetry and the associated P_D cannot have a sudden change (Fig. 3(e)). Hence, the unchanged defect symmetry and the associated P_D cause a reversible domain switching after removing E. Consequently, an interesting macroscopic double P–E loop and a large recoverable electrostrain curve are produced as in Fig. 2. For the fresh samples, since the defect symmetry is a cubic symmetry and cannot provide such an intrinsic restoring force, we can only observe a normal macroscopic P–E loop and a butterfly electrostrain curve due to the irreversible domain switching (Fig. 2(a)).

It should be noted that the microscopic description for the orthorhombic $KNbO_3$-based ferroelectrics is very similar to that for acceptor-doped tetragonal ferroelectric titanates [5–7]. The observed aging effects originate essentially from the inconformity of the crystal symmetry with the defect symmetry after a structural transition. This may be the intrinsic reason why macroscopic double P–E loops and recoverable electrostrains are achieved in

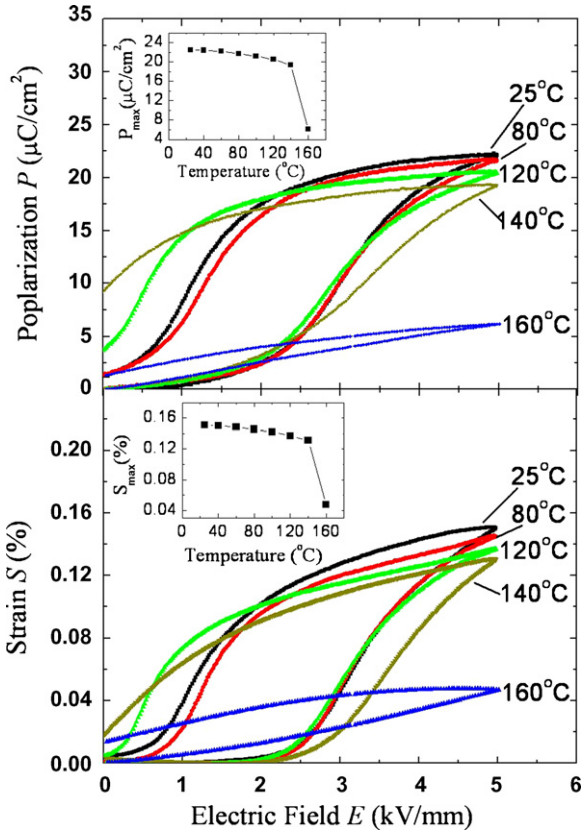

Fig. 4. Unipolar ferroelectric hysteresis (P–E) loops and electrostrain curves for the aged samples at different temperatures of 25, 80, 120, 140, and 160 °C. The inset shows the temperature dependence of maximum polarization P_{max} and maximum strain S_{max} of the aged samples at 5 kV/mm.

different ferroelectric phases and different ferroelectrics. Such aging mechanism, based on the SC-SRO principle of point defects, is insensitive to crystal symmetry and constituent ionic species, indicating a common physical origin of aging.

Fig. 4 plots the unipolar ferroelectric hysteresis (P–E) loops and electrostrain curves for the aged samples at different temperatures of 25, 80, 120, 140, and 160 °C in order to investigate their temperature stabilities for applications. The inset shows the temperature dependence of maximum polarization P_{max} and maximum strain S_{max} of the aged samples at 5 kV/mm. It can be seen that the aging-induced high P_{max} of >19 μC/cm^2 and large S_{max} of >0.13% can be persisted up to 140 °C, reflecting a good temperature stability for the effects. Above 140 °C, the unipolar P–E loop and the electrostrain curve become normal, while P_{max} and S_{max} decrease significantly. This can be ascribed to the destruction of defect symmetry and migration of V_O as a result of the exposure to high temperature and the approach of the tetragonal phase (T_{O-T} = 148 °C). Thus, point defects cannot provide a restoring force for a reversible domain switching so that the obvious P–E loop becomes a normal loop and the recoverable electrostrain curve vanishes.

In summary, we have investigated the aging-induced double P–E loops and recoverable electrostrain curves in an Mn-doped orthorhombic $KNbO_3$-based [$K(Nb_{0.90}Ta_{0.10})O_3$] lead-free ceramic: $K[(Nb_{0.90}Ta_{0.10})_{0.99}Mn_{0.01}]O_3$. It has been observed that aging in the orthorhombic ferroelectric state induces a double P–E loop and a large recoverable electrostrain of 0.15% at 5 kV/mm. Such aging effects in the orthorhombic samples have been explained by a point defect-mediated reversible domain switching mechanism of aging driven by a symmetry-conforming short-range ordering (SC-SRO) of point defects. Large nonlinear electrostrain of >0.13% in a broad temperature range of 25–140 °C has suggested potential applications of the aging effects to enhance the electromechanical properties of environmental-friendly (lead-free) ceramics.

Acknowledgment

This work was supported by the Innovation and Technology Fund of the HKSAR under Grant No. GHP/003/06.

References

[1] B. Jaffe, W.R. Cook, H. Jaffe, Piezoelectric Ceramics, Academic, New York, 1971.
[2] P.V. Lambeek, G.H. Jonker, J. Phys. Chem. Solids 47 (1986) 453.
[3] W.A. Schulze, K. Ogino, Ferroelectrics 87 (1988) 361.
[4] K. Uchino, Ferroelectric Device, Dekker, New York, 2000, p. 279.
[5] X. Ren, Nat. Mater. 3 (2004) 91.
[6] L.X. Zhang, X. Ren, Phys. Rev. B 71 (2005) 174108.
[7] L.X. Zhang, X. Ren, Phys. Rev. B 73 (2006) 094121.
[8] D. Damjanovic, Rep. Prog. Phys. 61 (1998) 1267.
[9] G. Arlt, U. Rebels, Integr. Ferroelectr. 3 (1993) 343.
[10] D.A. Hall, M.M. Ben-Omran, J. Phys.: Condens. Matter 10 (1998) 9129.
[11] K. Okasaki, K. Sakata, Electrotech. J. Jpn. 7 (1962) 13.
[12] M. Takahashi, Jpn. J. Appl. Phys. 9 (1970) 1236.
[13] K. Carl, K.H. Hardtl, Ferroelectrics 17 (1978) 473.
[14] U. Robels, G. Arlt, J. Appl. Phys. 73 (1993) 3454.
[15] P.V. Lambeck, G.H. Jonker, Ferroelectrics 22 (1978) 729.
[16] G.L. Yuen, Y. Yang, S.W. Or, Appl. Phys. Lett. 91 (2007) 122907.
[17] X.X. Wang, S.W. Or, K.H. Lam, H.L.W. Chan, P.K. Choy, P.C.K. Liu, J. Electroceram. 16 (2006) 385.
[18] K. Yamanouchi, H. Odagawa, T. Kojima, T. Matsumura, Electron. Lett. 33 (1997) 193.
[19] Y. Saito, H. Takao, T. Tani, T. Nonoyama, K. Takatori, T. Homma, T. Nagaya, M. Nakamura, Nature (Lond.) 42 (2004) 84.
[20] S. Triebwasser, Phys. Rev. 114 (1959) 63.
[21] S.-E. Park, T.R. Shrout, J. Appl. Phys. 82 (1997) 1804.
[22] Z. Feng, X. Ren, Appl. Phys. Lett. 91 (2007) 032904.
[23] X. Ren, K. Otsuka, Phys. Rev. Lett. 85 (2000) 1016.